Journal of Sound and Vibration (2002) **257**(4), 733–752
doi:10.1006/jsvi.5041, available online at http://www.idealibrary.com on IDEAL®

LARGEST LYAPUNOV EXPONENT AND ALMOST CERTAIN STABILITY ANALYSIS OF SLENDER BEAMS UNDER A LARGE LINEAR MOTION OF BASEMENT SUBJECT TO NARROWBAND PARAMETRIC EXCITATION

Z. H. Feng and H. Y. Hu

Institute of Vibration Engineering Research, Nanjing University of Aeronautics and Astronautics, 210016 *Nanjing, People's Republic of China. E-mail: uusw@public*1.*sz.js.cn*

(*Received* 13 *August* 2001, *and in final form* 17 *December* 2001)

The first order approximate solutions of a set of non-liner differential equations, which is established by using Kane's method and governs the planar motion of beams under a large linear motion of basement, are systematically derived via the method of multiple scales. The non-linear dynamic behaviors of a simply supported beam subject to narrowband random parametric excitation, in which either the principal parametric resonance of its first mode or a combination parametric resonance of the additive type of its first two modes with or without 3:1 internal resonance between the first two modes is taken into consideration, are analyzed in detail. The largest Lyapunov exponent is numerically obtained to determine the almost certain stability or instability of the trivial response of the system and the validity of the stability is verified by direct numerical integration of the equation of motion of the system.

1. INTRODUCTION

Flexible structures undergoing a large linear motion and undertaking both constant and random pulsating thrust are widely used in the fields of aviation engineering, military engineering and so on. However, it is far from an easy task to gain an insight into the dynamics of a flexible structure, even a slender beam, which is one of the simplest flexible structures, owing to the complicated non-linear dynamics by nature. Recently, Feng and Hu [1, 2] established a set of non-linear differential equations by using Kane's method for the planar oscillation of slender beams subject to a parametric excitation of the base movement, with the cubic non-linearities of geometrical and inertia types taken into consideration. In reference [2], the complicated non-linear dynamic behaviors of a slender simply supported beam with principal parametric and 3:1 internal resonances were systematically investigated and the corresponding parametrically excited dynamic stability was analyzed in detail. As the parametric excitation, however, was restricted to be deterministic, the significance of random parametric excitation, especially narrowband random parametric excitation, has not been highlighted.

References to narrowband random excitation oscillators are few up to now. Rajan and Davies [3] considered the random primary response of a Duffing oscillator subject to narrowband excitation by using the method of multiple scales and stochastic averaging. At the same time, Davies and Rajan [4] investigated the random superharmonic and

0022-460X/02/$35.00

subharmonic responses of the same oscillator stated above to narrowband excitation by using the same two approaches. Nayfeh and Serhan [5] analyzed the stationary mean and mean square responses and their local stability of a Duffing–Rayleigh oscillator excited by the sum of a deterministic harmonic component and a random component by using a second order closure method. Zhu *et al.* [6] numerically investigated the stochastic jump and bifurcation of a Duffing oscillator under the external narrowband excitation. Zhu [7] thought that the study of the random parametrically excited systems was more important than that of random externally excited ones and was more difficult in theory. Recently, Rong *et al.* [8, 9] studied the principal resonance of a Duffing oscillator to combined deterministic and narrowband parametric excitations via the method of multiple scales. The non-linear dynamic behaviors such as stability and bifurcation of the steady response were systematically investigated in their studies. However, related research objects are mainly concentrated on some classical modes such as Duffing oscillator, and objects with engineering significance have been rarely dealt with so far.

The aim of this paper is to reveal the non-linear dynamics of slender beams subject to both a large linear motion and a small narrowband random excitation of basement. In what follows, the random component is taken to be harmonic having a random amplitude and phase. The paper is organized as follows. The non-linear dynamic equations of planar motion are derived for the slender beams via Kane's method in section 2. In section 3, the method of multiple scales is used to determine the modulation of amplitude and phase of a simply supported beam. In section 4, some non-linear dynamic behaviors of the system without any internal resonances are discussed. The largest Lyapunov exponent of the trivial response and its corresponding stability of the system to either the narrowband random principal parametric resonance of the first mode or the combination random parametric resonance of the first two modes are studied by means of qualitative analyses. Also, in section 5, the largest Lyapunov exponent of the trivial response and its stability of the system to the combination of principal narrowband random parametric resonance of the first mode and the 3:1 internal resonance of the first two modes are systematically analyzed. Finally, some conclusions are drawn in section 6.

2. EQUATIONS OF MOTION

As shown in Figure 1, a slender uniform beam B is simply supported on a rigid basement A, which is moving along in $\mathbf{r}_0$ with respect to the Newtonian reference frame N fixed on the ground. The beam is characterized by the natural length l, the area of cross-section A_0, the second moment of area of cross-section I, the mass per unit length ρ, and Young's modulus E.

To describe the motion of the beam, two unit vectors $\mathbf{a}_1$ and $\mathbf{a}_2$ are defined in Figure 1, where $\mathbf{a}_1$ is parallel to the centroidal axis of the underformed beam, while $\mathbf{a}_2$ is parallel to the central principal axis of the cross-section of the beam. Both are fixed in the relative reference frame R_1 built into the basement A.

The kinetic description of the beam can be made through an arbitrary, infinitely short element of the beam, which has a distance x away from point O. For the slender beam, the motion of such an element can be fully determined by the point C_v at the centroidal axis of the beam. When the beam is deformed due to the motion of the basement and any other disturbance, the point C_v moves to point C, positioned by a vector $\mathbf{u}$ to describe the relatively elastic deformation of C_v.

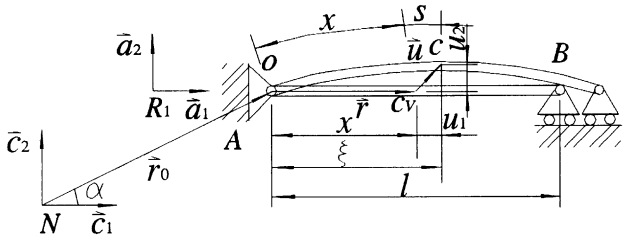

Figure 1. Configuration of a simply supported beam in a large linear motion.

Following references [1, 2] and neglecting the rotary inertia, transverse shear and torsion of slender beams, one can derive the following geometric relation:

$$x + s = \int_0^x \sqrt{(1 + u_{1,\beta})^2 + (u_{2,\beta})^2}\, \mathrm{d}\beta, \tag{1}$$

where $u_{1,\beta}$ and $u_{2,\beta}$ are the partial derivatives of u_1 and u_2 with respect to the dummy variable β, i.e., the distance from point C_v to point O. In what follows, the deformation of the beam is assumed to be not very large. By means of the truncated Taylor expansion under this assumption, equation (1) can be approximated as

$$u_1 = s - \frac{1}{2}\int_0^x (u_{2,\beta})^2\, \mathrm{d}\beta. \tag{2}$$

To simplify the partial differential equations of the beam into a set of ordinary differential equations, the Rayleigh–Ritz method is used to approximate the variables s and u_2 as follows:

$$s(x,t) = \sum_{i=1}^{n_1} \Phi_{1i}(x) q_i(t), \quad u_2(x,t) = \sum_{i=1}^{n_2} \Phi_{2i}(x) Q_i(t), \tag{3}$$

where Φ_{1i} and Φ_{2i} are the stretching and bending modal shapes of the beam when the basement is not moving, q_i and Q_i are the corresponding modal co-ordinates, and n_1 and n_2 are the numbers of modal co-ordinates used in the analysis.

According to references [1, 2], the axial load P and the moment of bending M of the beam can be simplified as follows:

$$P = EA_0 s_x, \quad M = EIu_{2,\xi\xi}(1 + u_{2,\xi}^2)^{-3/2}. \tag{4, 5}$$

In general, the strain energy of beam U can be given by

$$U = \int_0^l \frac{P^2}{2EA_0}\, \mathrm{d}x + \int_0^l \frac{M^2}{2EI}\, \mathrm{d}x. \tag{6}$$

Kane's method implies that the generalized inertial force of an infinitely short element of the beam should be balanced by the generalized active force on the same element of the beam, that is

$$\int_0^l \rho \left(\mathbf{a}_N^C \cdot \frac{\partial \mathbf{v}_N^C}{\partial \dot{y}_k} \right) \mathrm{d}x + \frac{\partial U}{\partial \dot{y}_k} = 0, \tag{7}$$

where y_k is either q_k or Q_k, $\mathbf{v}_N^C$ and $\mathbf{a}_N^C$ are the inertial velocity and acceleration of the center C respectively.

Using the orthogonality property between modal shapes Φ_{1i} and Φ_{1j} and the orthogonality property between modal shapes Φ_{2i} and Φ_{2j} for the undamped beam, one

can finally obtain

$$M_{1k}\ddot{q}_k + K_{1k}q_k - \sum_{i=1}^{n_2}\sum_{j=1}^{n_2}(2D_{1ij}^k + E_{1ij}^k)Q_iQ_j - \sum_{i=1}^{n_2}\sum_{j=1}^{n_2}C_{1ij}^k(\dot{Q}_i\dot{Q}_j + Q_i\ddot{Q}_j)$$
$$= -a_{1k}\dot{v}_0\cos\alpha, \quad k = 1, 2, \ldots, n_1, \tag{8}$$

$$M_{2k}\ddot{Q}_k + K_{2k}Q_k - \sum_{i=1}^{n_2}(a_{2i}^k\dot{v}_0\cos\alpha)Q_i - \sum_{i=1}^{n_1}\sum_{j=1}^{n_2}C_{2ij}^k\ddot{q}_iQ_j - \sum_{i=1}^{n_1}\sum_{j=1}^{n_2}(4E_{2ij}^{k1} + E_{2ij}^{k2} + E_{2ij}^{k3})q_iQ_j$$
$$+ \sum_{h=1}^{n_2}\sum_{i=1}^{n_2}\sum_{j=1}^{n_2}D_{2hij}^k(Q_hQ_i\ddot{Q}_j + Q_h\dot{Q}_i\dot{Q}_j) + \sum_{h=1}^{n_2}\sum_{i=1}^{n_2}\sum_{j=1}^{n_2}(F_{2ijh}^k + G_{2ijh}^k)Q_hQ_iQ_j$$
$$= -b_{2k}\dot{v}_0\sin\alpha, \quad k = 1, 2, \ldots, n_2, \tag{9}$$

where

$$M_{1k} = \int_0^l \rho\Phi_{1k}\Phi_{1k}\,\mathrm{d}x, \quad K_{1k} = \int_0^l EA_0\Phi_{1k,x}\Phi_{1k,x}\,\mathrm{d}x, \quad C_{1ij}^k = \int_0^l \phi_{ij}\Phi_{1k}\,\mathrm{d}x,$$
$$a_{1k} = \int_0^l \rho\Phi_{1k}\,\mathrm{d}x,$$
$$D_{1ij}^k = \int_0^l EI\Phi_{2i,xx}\Phi_{2j,xx}\Phi_{1k,x}\,\mathrm{d}x, \quad E_{1ij}^k = \int_0^l EI\Phi_{2i,xx}\Phi_{2j,x}\Phi_{1k,xx}\,\mathrm{d}x, \quad a_{2i}^k = \int_0^l \rho\phi_{ik}\,\mathrm{d}x,$$
$$M_{2k} = \int_0^l \rho\Phi_{2k}\Phi_{2k}\,\mathrm{d}x, \quad K_{2k} = \int_0^l EI\Phi_{2k,xx}\Phi_{2k,xx}\,\mathrm{d}x, \quad C_{2ij}^k = \int_0^l \rho\Phi_{1i}\phi_{ij}\,\mathrm{d}x,$$
$$D_{2hij}^k = \int_0^l \rho\phi_{ij}\phi_{hk}\,\mathrm{d}x, \quad E_{2ij}^{k1} = \int_0^l EI\Phi_{2j,xx}\Phi_{2k,xx}\Phi_{1i,x}\,\mathrm{d}x, \; E_{2ij}^{k2} = \int_0^l EI\Phi_{1j,xx}\Phi_{2i,x}\Phi_{2k,xx}\,\mathrm{d}x,$$
$$E_{2ij}^{k3} = \int_0^l EI\Phi_{1j,xx}\Phi_{2i,xx}\Phi_{2k,x}\,\mathrm{d}x, \; F_{2ijh}^k = \int_0^l EI\Phi_{2i,xx}\Phi_{2k,xx}\Phi_{2j,x}\Phi_{2h,x}\,\mathrm{d}x, \quad b_{2k} = \int_0^l \rho\Phi_{2k}\,\mathrm{d}x$$
$$G_{2ijh}^k = \int_0^l EI\Phi_{2i,xx}\Phi_{2j,xx}\Phi_{2h,x}\Phi_{2k,x}\,\mathrm{d}x, \quad \phi_{ij} = \int_0^x \Phi_{2i,\beta}(\beta)\Phi_{2j,\beta}(\beta)\,\mathrm{d}\beta$$

3. FIRST ORDER APPROXIMATE SOLUTION

In what follows, the cases of a simply supported slender beam and $\alpha = 0$ are taken into consideration. Assume that the base acceleration is not very large and the stretch of the arc length of the beam is so small that the beam can be treated as an inextensional one. To arrive at general results and conclusions, a few dimensionless variables are introduced as the following:

$$\eta = \frac{x}{l}, \quad \tau = \frac{\pi^2 t}{T}, \quad \vartheta_k = \frac{Q_k}{\lambda l}, \tag{10}$$

where $T = \sqrt{\rho l^4/EI}$ and $\tilde{\lambda}$ represents a scaling factor.

In what follows, the motion of the basement is assumed to be

$$\dot{v}_0 = a_0 + \xi(t), \tag{11}$$

where a_0 is the average acceleration and $\xi(t)$ a narrowband random process which has the same form as that described in references [3–5, 8–10] and is given by

$$\xi(t) = f\cos\omega_c t + g\sin\omega_c t, \tag{12}$$

where ω_c is the center frequency of $\xi(t)$, and f and g are slowly varying stationary random processes with zero means. Here $\xi(t)$ is chosen to be a zero-mean Gaussian narrowband random excitation. It could be obtained by filtering a white noise through a linear filter [3–5, 10], that is

$$\ddot{\xi} + \omega_c^2 \xi + \gamma \dot{\xi} = \gamma^{1/2} \omega_c W, \tag{13}$$

where γ stands for the bandwidth of the filter. The autocorrelation function of the white noise W is given by

$$R_W(t) = 2\pi S_0 \delta(\tau), \tag{14}$$

where S_0 is the spectrum constant of W and δ the Dirac delta function. The spectrum of ξ is given by

$$\frac{\gamma \omega_c^2 S_0}{(\omega_c^2 - \omega^2)^2 + \gamma^2 \omega^2} \to \pi S_0 \delta(\omega_c), \quad \gamma \to 0. \tag{15}$$

Substituting equation (12) into equation (13) and performing deterministic and stochastic averaging of the equations describing the modulations of f and g, one obtains

$$\dot{f} = (\gamma/2)^{1/2} W_c - (\gamma/2) f, \quad \dot{g} = (\gamma/2)^{1/2} W_s - (\gamma/2) g. \tag{16}$$

The white noise components W_c and W_s are independent and their autocorrelation functions are given by equation (14) and have the following forms:

$$R_f(\tau) = R_g(\tau) = \pi S_0 \mathrm{e}^{-\gamma|\tau|/2}. \tag{17}$$

The correlation time of f and g is $O(1/\gamma)$. This means that for sufficiently small bandwidth, f and g are slowly varying functions of time.

Substituting equations (10)–(12) into equation (9) yields

$$\ddot{\vartheta}_k + (\tilde{\omega}_k^2 - a_{2k}^k)\vartheta_k - \sum_{\substack{i=1 \\ i \neq k}}^{n_2} a_{2i}^k \vartheta_i - \varepsilon \sum_{i=1}^{n_2} (f_{2i}^k \cos \omega\tau + g_{2i}^k \sin \omega\tau)\vartheta_i + \varepsilon \sum_{i=1}^{n_2}\sum_{j=1}^{n_2}\sum_{h=1}^{n_2} \alpha_{ijh}^k \vartheta_i \vartheta_j \vartheta_h$$
$$+ \varepsilon \sum_{i=1}^{n_2}\sum_{j=1}^{n_2}\sum_{h=1}^{n_2} \beta_{ijh}^k \vartheta_i (\dot{\vartheta}_j \dot{\vartheta}_h + \vartheta_j \ddot{\vartheta}_h) = 0, \quad k = 1, 2, \ldots, n_2, \tag{18}$$

where

$$\tilde{\omega}_k^2 = \tilde{K}_{2k}/\tilde{M}_{2k}, \quad \omega = \omega_c T/\pi^2, \quad a_{2i}^k = a_0 T^2 \tilde{a}_{2i}^k / l\pi^4 \tilde{M}_{2k}, \quad f_{2i}^k = f T^2 \tilde{a}_{2i}^k / \varepsilon l \pi^4 \tilde{M}_{2k},$$
$$g_{2i}^k = g T^2 \tilde{a}_{2i}^k / \varepsilon l \pi^4 \tilde{M}_{2k}, \quad \alpha_{ijh}^k = \tilde{\alpha}_{ijh}^k / \varepsilon \tilde{M}_{2k}, \quad \beta_{ijh}^k = \tilde{\beta}_{ijh}^k / \varepsilon \tilde{M}_{2k}, \quad \tilde{C}_{2k} = C_{2k} T/\pi^2 \rho l,$$
$$\tilde{K}_{2k} = (1/\pi^4) \int_0^1 \Phi_{2k,\eta\eta}^2 \, \mathrm{d}\eta, \quad \tilde{\beta}_{ijh}^k = \bar{\lambda}^2 \int_0^1 \phi_{ij} \phi_{hk} \, \mathrm{d}\eta, \quad \phi_{ij} = \int_0^\eta \Phi_{2i,\beta} \Phi_{2j,\beta} \, \mathrm{d}\beta, \quad \tilde{M}_{2k} = \int_0^1 \Phi_{2k}^2 \, \mathrm{d}\eta,$$
$$\tilde{a}_{2i}^k = \int_0^1 \phi_{ik} \, \mathrm{d}\eta, \quad \tilde{\alpha}_{ijh}^k = (\bar{\lambda}^2/\pi^4) \int_0^1 \Phi_{2i,\eta\eta} \Phi_{2j,\eta} (\Phi_{2h,\eta\eta} \Phi_{2k,\eta} + \Phi_{2h,\eta} \Phi_{2k,\eta\eta}) \, \mathrm{d}\eta, \quad 0 < \varepsilon \ll 1.$$

Decoupling equation (18) through the use of linear transformation $\vartheta = \Phi y$, where $\vartheta = \{\vartheta_1 \vartheta_2 \cdots \vartheta_{n_2}\}^{\mathrm{T}}$, $y = \{y_1 y_2 \cdots y_{n_2}\}^{\mathrm{T}}$, and $\Phi = \{\varphi_1 \varphi \cdots \varphi_{n_2}\}$ is the normalized mode matrix of linearized equation (18), and introducing the viscous modal damping to characterize the energy dissipation, one has

$$\ddot{y}_k + 2\varepsilon \hat{\zeta}_k \dot{y}_k + \omega_k^2 y_k - \varepsilon \sum\nolimits_{i=1}^{n_2} (\hat{f}_{2i}^k \cos \omega\tau + \hat{g}_{2i}^k \sin \omega\tau) y_i + \varepsilon \sum\nolimits_{i=1}^{n_2} \sum\nolimits_{j=1}^{n_2} \sum\nolimits_{h=1}^{n_2} \hat{\alpha}_{ijh}^k y_i y_j y_h$$
$$+ \varepsilon \sum\nolimits_{i=1}^{n_2} \sum\nolimits_{j=1}^{n_2} \sum\nolimits_{h=1}^{n_2} \hat{\beta}_{ijh}^k (\dot{y}_j \dot{y}_h + y_j \ddot{y}_h) = 0, \quad k = 1, 2, \ldots, n_2, \tag{19}$$

where $\hat{f}_{2i}^{k} = \sum_{p=1}^{n_2}\sum_{h=1}^{n_2}\varphi_{pk}f_{2h}^{p}\varphi_{hi}$, $\hat{g}_{2i}^{k} = \sum_{p=1}^{n_2}\sum_{h=1}^{n_2}\varphi_{pk}g_{2h}^{p}\varphi_{hi}$, $\hat{\alpha}_{ijh}^{k} = \sum_{p=1}^{n_2}\sum_{l=1}^{n_2}\sum_{m=1}^{n_2}\sum_{n=1}^{n_2}\varphi_{pk}\alpha_{lmn}^{p}\varphi_{li}\varphi_{mi}\varphi_{nh}$, and $\hat{\beta}_{ijh}^{k} = \sum_{p=1}^{n_2}\sum_{l=1}^{n_2}\sum_{m=1}^{n_2}\sum_{n=1}^{n_2}\varphi_{pk}\beta_{lmn}^{p}\varphi_{li}\varphi_{mj}\varphi_{nh}$.

The first two sets of coefficients stated above give the amplitudes of narrowband random parametric excitation and the last two sets the non-linear interaction coefficients between the modal co-ordinates.

The method of multiple scales has been widely used in the analysis of deterministic systems. However, Rajan and Davies [3], Davies and Rajan [4], Nayfeh and Serhan [5], and Rong *et al.* [8, 9] extend this method to the analysis of non-linear systems subject to random external or parametric excitations. Here, now, this method is also used to derive the first order approximate solutions of equation (19) as the following:

$$y_k(\tau,\varepsilon) = y_{k0}(T_0,T_1) + \varepsilon y_{k1}(T_0,T_1), \tag{20}$$

where $T_0 = \tau$, $T_1 = \varepsilon\tau$, and $k = 1,2,\ldots,n_2$. Substituting the solution candidates into equation (19) and equation the coefficients of some powers of ε, one obtains

$$D_0^2 y_{k0} + \omega_k^2 y_{k0} = 0, \quad k = 1,2,\ldots,n_2, \tag{21a}$$

$$\begin{aligned} &D_0^2 y_{k1} + \omega_k^2 y_{k1} = -2\hat{\varsigma}_k D_0 y_{k0} - 2D_0 D_1 y_{k0} + \sum_{i=1}^{n_2}(\hat{f}_{2i}^{k}\cos\omega\tau + \hat{g}_{2i}^{k}\sin\omega\tau)y_{i0} \\ &- \sum_{i=1}^{n_2}\sum_{j=1}^{n_2}\sum_{h=1}^{n_2}\hat{\alpha}_{ijh}^{k}y_{i0}y_{j0}y_{h0} - \sum_{i=1}^{n_2}\sum_{j=1}^{n_2}\sum_{h=1}^{n_2}\hat{\beta}_{ijh}^{k}y_{i0}(D_0 y_{j0}D_0 y_{h0} + y_{j0}D_0^2 y_0), \\ &k = 1,2,\ldots,n_2, \end{aligned} \tag{21b}$$

where $D_0 = \partial/\partial T_0$ and $D_1 = \partial/\partial T_1$ are the partial differential operators.

The solution of linear partial differential equation (21a) can be written in the complex form

$$y_{k0} = A_k(T_1)\exp(\mathrm{i}\omega_k T_0) + \text{c.c.}, \quad k = 1,2,\ldots,n_2, \tag{22}$$

where c.c. stands for the complex conjugate of the preceding terms. Substituting equation (22) into equation (21b) yields

$$\begin{aligned} D_0^2 y_{k1} + \omega_k^2 y_{k1} = &-2\mathrm{i}\omega_k(\hat{\varsigma}_k A_k + A_k')\exp(\mathrm{i}\omega_k T_0) \\ &+ \frac{1}{2}\sum_{m=1}^{n_2}(\hat{f}_{2m}^{k} - \mathrm{i}g_{2m}^{k})\{A_m\exp[\mathrm{i}(\omega+\omega_m)\tau] + \bar{A}_m\exp[\mathrm{i}(\omega-\omega_m)\tau]\} \\ &+ \sum_{m=1}^{n_2}\sum_{j=1}^{n_2}\sum_{h=1}^{n_2}\{(-\hat{\alpha}_{mjh}^{k} + \omega_j\omega_h\hat{\beta}_{mjh}^{k} + \omega_h^2\hat{\beta}_{mjh}^{k}) \\ &A_m A_j A_h\exp[\mathrm{i}(\omega_m+\omega_j+\omega_h)\tau] \\ &+ (-\hat{\alpha}_{mjh}^{k} - \omega_j\omega_h\hat{\beta}_{mjh}^{k} + \omega_h^2\hat{\beta}_{mjh}^{k})A_m\bar{A}_j A_h\exp[\mathrm{i}(\omega_m-\omega_j+\omega_h)\tau] \\ &+ (-\hat{\alpha}_{mjh}^{k} + \omega_j\omega_h\hat{\beta}_{mjh}^{k} + \omega_h^2\hat{\beta}_{mjh}^{k})\bar{A}_m A_j A_h\exp[\mathrm{i}(-\omega_m+\omega_j+\omega_h)\tau] \\ &+ (-\hat{\alpha}_{mjh}^{k} - \omega_j\omega_h\hat{\beta}_{mjh}^{k} + \omega_h^2\hat{\beta}_{mjh}^{k})\bar{A}_m\bar{A}_j A_h\exp[\mathrm{i}(-\omega_m-\omega_j+\omega_h)\tau]\} \\ &+ \text{c.c.}, \quad k = 1,2,\ldots,n_2, \end{aligned} \tag{23}$$

where the overbar stands for the complex conjugate.

A particular solution of equation (23) may contain some secular terms and small-divisor terms because of the presence of principal parametrical resonance or combination parametric resonance or internal resonance between the natural modes. In what follows, only two natural modes are taken into consideration to investigate the behaviors of random parametric resonances.

4. RANDOM PRINCIPAL AND COMBINATION PARAMETRIC RESONANCES WITHOUT ANY INTERNAL RESONANCES

Assume that there exist no internal resonances between any two natural modes. In order to investigate the random combination parametric resonance between the mth and the nth natural modes, the frequency detuning parameter σ_1 is introduced as given below:

$$\omega = \omega_m + \omega_n + \varepsilon\sigma_1, \quad m, n = 1, 2, \ldots, n_2. \tag{24}$$

Substituting this equation into equation (23) and eliminating the terms that produce secular terms in y_{k1}, one obtains

$$\begin{aligned}
&2\mathrm{i}\omega_m(\hat{\varsigma}_m A_m + A_m') - \tfrac{1}{2}(\hat{f}_{2n}^m - \mathrm{i}\hat{g}_{2n}^m)\bar{A}_n \exp(\mathrm{i}\sigma_1 T_1) + \sum\nolimits_{j=1}^{n_2} c_{mj} A_j \bar{A}_j A_m = 0,\\
&2\mathrm{i}\omega_n(\hat{\varsigma}_n A_n + A_n') - \tfrac{1}{2}(\hat{f}_{2m}^n - \mathrm{i}\hat{g}_{2m}^n)\bar{A}_m \exp(\mathrm{i}\sigma_1 T_1) + \sum\nolimits_{j=1}^{n_2} c_{nj} A_j \bar{A}_j A_n = 0,\\
&2\mathrm{i}\omega_k(\hat{\varsigma}_k A_k + A_k') + \sum\nolimits_{j=1}^{n_2} c_{kj} A_j \bar{A}_j A_k = 0, \quad k \neq m, n,
\end{aligned} \tag{25}$$

where

$$c_{kj} = \begin{cases} 3\hat{\alpha}_{kkk}^k - 2\omega_k^2 \hat{\beta}_{kkk}^k, & j = k,\\ 2(\hat{\alpha}_{kjj}^k + \hat{\alpha}_{jjk}^k + \hat{\alpha}_{jkj}^k - \omega_j^2 \hat{\beta}_{jkj}^k - \omega_k^2 \hat{\beta}_{jjk}^k), & j \neq k. \end{cases}$$

As the modes for $k \neq m, n$ are neither directly excited by the external excitation, nor indirectly excited by the internal resonance, only the mth and the nth natural modes contribute to the steady state response due to the presence of viscous damping. Finally, one has

$$\begin{aligned}
&2\mathrm{i}\omega_m(\hat{\varsigma}_m A_m + A_m') - \tfrac{1}{2}(\hat{f}_{2n}^m - \mathrm{i}\hat{g}_{2n}^m)\bar{A}_n \exp(\mathrm{i}\sigma_1 T_1) + c_{mn} A_n \bar{A}_n A_m + c_{mm} A_m^2 \bar{A}_m = 0,\\
&2\mathrm{i}\omega_n(\hat{\varsigma}_n A_n + A_n') - \tfrac{1}{2}(\hat{f}_{2m}^n - \mathrm{i}\hat{g}_{2m}^n)\bar{A}_m \exp(\mathrm{i}\sigma_1 T_1) + c_{nn} A_n^2 \bar{A}_n + c_{nm} A_m \bar{A}_m A_n = 0.
\end{aligned} \tag{26}$$

Similarly, to describe the closeness of the beam to the random principal parametric resonance of the mth natural mode, the frequency detuning parameter σ_1 is also introduced as given below:

$$\omega = 2\omega_m + \varepsilon\sigma_1, \quad m = 1, 2, \ldots, n_2. \tag{27}$$

Substituting the above equation into equation (23) and eliminating the terms that produce secular terms in y_{k1}, one finally has

$$2\mathrm{i}\omega_m(\hat{\varsigma}_m A_m + A_m') - \tfrac{1}{2}(\hat{f}_{2m}^m - \mathrm{i}\hat{g}_{2m}^m)\bar{A}_m \exp(\mathrm{i}\sigma_1 T_1) + c_{mm} A_m^2 \bar{A}_m = 0. \tag{28}$$

In what follows, without loss of generality, only the first two natural modes are involved to investigate the random parametric resonances.

4.1. RANDOM PRINCIPAL PARAMETRIC RESONANCE OF THE FIRST NATURAL MODE

4.1.1. *Modulation equations and the largest Lyapunov exponent*

Following equation (28), the condition of random principal parametric resonance of the first natural mode holds true when $m = 1$, that is $\omega = 2\omega_1 + \varepsilon\sigma_1$. Consequently, one has

$$\mathrm{i}\omega_1(\hat{\varsigma}_1 A_1 + A_1') - \tfrac{1}{4}(\hat{f}_{21}^1 - \mathrm{i}\hat{g}_{21}^1)\bar{A}_1 \exp(\mathrm{i}\sigma_1 T_1) + \tfrac{1}{2} c_{11} A_1^2 \bar{A}_1 = 0. \tag{29}$$

Substituting the Cartersian transformation

$$A_1(T_1) = \tfrac{1}{2}[U_1(T_1) - \mathrm{i}V_1(T_1)]\,\mathrm{e}^{\mathrm{i}\lambda_1}, \quad \lambda_1 = \frac{\sigma_1}{2}T_1 \tag{30}$$

into equation (29) and separating the results into real and imaginary parts, one arrives at a set of ordinary differential equations, namely, the modulation equations of steady state response

$$\begin{aligned} U_1' &= \left(-\hat{\varsigma}_1 - \frac{\hat{g}_{21}^1}{4\omega_1}\right)U_1 + \left(-\frac{\sigma_1}{2} + \frac{\hat{f}_{21}^1}{4\omega_1}\right)V_1 + \frac{1}{8\omega_1}c_{11}(U_1^2 + V_1^2)\,V_1, \\ V_1' &= \left(\frac{\sigma_1}{2} + \frac{\hat{f}_{21}^1}{4\omega_1}\right)U_1 + \left(-\hat{\varsigma}_1 + \frac{\hat{g}_{21}^1}{4\omega_1}\right)V_1 - \frac{1}{8\omega_1}c_{11}(U_1^2 + V_1^2)U_1. \end{aligned} \tag{31}$$

In what follows, the analysis is mainly focused on the stability of the trivial response of equation (31). To obtain the necessary and sufficient almost certain stability condition of equation (31), according to reference [9], one has the linearized part of the equation in the neighborhood of (0, 0):

$$\begin{aligned} U_1' &= \left(-\hat{\varsigma}_1 - \frac{\hat{g}_{21}^1}{4\omega_1}\right)U_1 + \left(-\frac{\sigma_1}{2} + \frac{\hat{f}_{21}^1}{4\omega_1}\right)V_1, \\ V_1' &= \left(\frac{\sigma_1}{2} + \frac{\hat{f}_{21}^1}{4\omega_1}\right)U_1 + \left(-\hat{\varsigma}_1 + \frac{\hat{g}_{21}^1}{4\omega_1}\right)V_1. \end{aligned} \tag{32}$$

For ergodic random processes f and g, according to Oseledec multiplicative ergodic theory, it can be concluded that for any initial value (U_{10}, V_{10}), the Lyapunov exponent of the phase portraits $(U_1(T_1, U_{10}, V_{10}), V_1(T_1, U_{10}, V_{10}))$ in equation (32) can be described as

$$\lambda(U_{10}, V_{10}) = \lim_{T_1\to\infty} \frac{1}{T_1} \ln[(U_1(T_1, U_{10}, V_{10}))^2 + (V_1(T_1, U_{10}, V_{10}))^2]^{1/2}. \tag{33}$$

From equation (33), one can obtain two different Lyapunov exponents. Thus, the almost stability of the trivial response of equation (31) can be determined by the largest Lyapunov exponent $\lambda = \lambda_{max}$, i.e., when $\lambda < 0$, the trivial solution is almost certainly stable and is unstable when $\lambda > 0$.

Alternatively, by using the following polar co-ordinate transformation

$$U_1 = r\cos\frac{\eta}{2}, \quad V_1 = r\sin\frac{\eta}{2}, \tag{34}$$

one can transform equation (32) to

$$\begin{aligned} r' &= -\hat{\varsigma}_1 r + \frac{r}{4\omega_1}(\hat{f}_{21}^1 \sin\eta - \hat{g}_{21}^1 \cos\eta), \\ \eta' &= \sigma_1 + \frac{1}{2\omega_1}(\hat{f}_{21}^1 \cos\eta + \hat{g}_{21}^1 \sin\eta). \end{aligned} \tag{35}$$

By letting $\rho = \ln r$ and substituting it into equation (35), one obtains

$$\begin{aligned} \rho' &= -\hat{\varsigma}_1 + \frac{r}{4\omega_1}(\hat{f}_{21}^1 \sin\eta - \hat{g}_{21}^1 \cos\eta), \\ \eta' &= \sigma_1 + \frac{1}{2\omega_1}(\hat{f}_{21}^1 \cos\eta + \hat{g}_{21}^1 \sin\eta). \end{aligned} \tag{36}$$

Finally, one can evaluate the largest Lyapunov exponent by using another calculating form, that is

$$\lambda = -\hat{\varsigma}_1 + \frac{1}{4\omega_1}\lim_{T_1\to\infty}\frac{1}{T}\int_0^T [f_{21}^1(T_1)\sin\eta(T_1) - \hat{g}_{21}^1(T_1)\cos\eta(T_1)]\,\mathrm{d}T_1. \tag{37}$$

Obviously, equation (37) shows that the largest Lyapunov exponent is inversely proportional to the modal damping coefficient $\hat{\varsigma}_1$, i.e., the higher is the value of $\hat{\varsigma}_1$, the smaller is the value of λ.

4.1.2. *Numerical simulation of the largest Lyapunov exponent*

To understand the non-linear dynamics of slender beams subject to the combination of a large deterministic linear motion and a small narrowband random excitation, a few case studies at different basement movements will be given in this and the following sections. For this purpose, the dimensionless average acceleration $a = -a_0T^2/(\pi^4 l)$ and the dimensionless narrow band random process $\xi_1 = \xi T^2/(\pi^4 l)$ are introduced and the corresponding dimensionless slowly varying stationary random processes become $f_1 = fT^2/\pi^4 l$ and $g_1 = gT^2/\pi^4 l$, respectively, while the parameters ε and $\bar{\lambda}$ are fixed to 0·1 and 0·01 respectively. In Figure 2, the first order natural frequency, the second order natural frequency and the tripled first order natural frequency are shown as the functions in a. This figure enables one to perfectly tune a 3:1 internal resonance of the beam when $a = 0{\cdot}3160$.

Following references [3, 4, 8–10], for numerical simulation it is more convenient to use a pseudo-random signal given by

$$\xi_1(t) = \sqrt{\frac{2\sigma_\xi^2}{N}}\sum_{k=1}^{N}\cos(\omega_k t + \varphi_k). \tag{38}$$

The frequencies ω_k are chosen independently from a random population with probability density function of the same form as the spectrum of ξ_1, and the random phases φ_k are independent and uniformly distributed in $(0, 2\pi)$. Shinozuka [11] has verified that $\xi_1(t)$ tends to a Gaussian process as $N \to \infty$. For the very narrowband simulations used here, the spectrum chosen is a simple top-hat type, and the random frequencies are distributed uniformly in $(\omega - \gamma/2, \omega + \gamma/2)$. According to reference [9], f_1 and g_1, can be

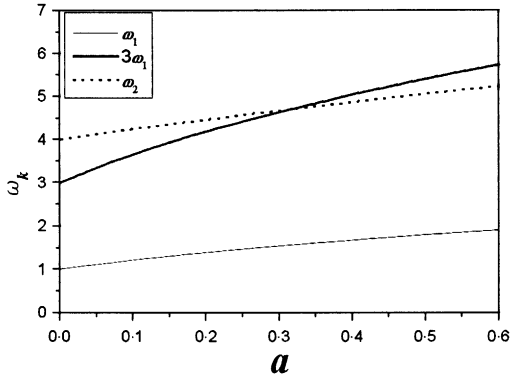

Figure 2. Variation of the first order natural frequency ω_1, the second order natural frequency ω_2 and the tripled first order natural frequency $3\omega_1$, with the dimensionless average acceleration a.

written as

$$f_1(T_1) = \sqrt{\frac{2\sigma_\xi^2}{N}} \sum_{k=1}^{N} \cos\left(\frac{\gamma}{\varepsilon}\Omega_k T_1 + \varphi_k\right),$$

$$g_1(T_1) = \sqrt{\frac{2\sigma_\xi^2}{N}} \sum_{k=1}^{N} \sin\left(\frac{\gamma}{\varepsilon}\Omega_k T_1 + \varphi_k\right), \tag{39}$$

where Ω_k are independent and uniformly distributed in $(-0{\cdot}5,\ 0{\cdot}5)$ and N is chosen as 500.

In the numerical simulation of this and the next section, a is fixed at 0·0912 and the corresponding parameters become $\omega_1 = 1{\cdot}2000$, $\omega_2 = 4{\cdot}2179$, $\hat{f}_{21}^1 = 49{\cdot}34 f_1$, and $\hat{g}_{21}^1 = 49{\cdot}34 g_1$ respectively. The time history of f_1 is shown in Figure 3. The variation of the largest Lyapunov exponent λ determined by equation (37) is shown in Figure 4(a) as $\lambda - (\sigma_1, \sigma_\xi^2)$ surface for the case of $\gamma = 0{\cdot}01$ and $\hat{\varsigma}_1 = 0{\cdot}1$. The corresponding isohypse curves of λ, which indirectly indicate the different almost certain stability boundaries of the trivial response for different damping parameters, are also shown in Figure 4(b). In other words, according to equation (37), for instance, the almost certain stability boundary is the isohypse curve of $\lambda = 0{\cdot}1$ when $\hat{\varsigma}_1 = 0{\cdot}2$, the isohypse curve of $\lambda = 0{\cdot}2$ when $\hat{\varsigma} = 0{\cdot}3$ and so on. When the value on the $\lambda - (\sigma_1, \sigma_\xi^2)$ surface is greater than zero, the corresponding trivial response is unstable; on the contrary, the response is stable. With the increase of γ from a small value, the stability of the trivial response of the system will change more or less. Figures 5(a) and 5(b) correspond to Figures 4(a) and 4(b) respectively. All parameters except the bandwidth of the narrow-band random excitation are kept the same: γ is increased from 0·01 to 0·1. It can be seen in Figure 5(a) that the mesh surface becomes flatter than that in Figure 4(a), which implies that the unstable areas will become narrower with the increase of γ and the isohypse curves in Figures 5(b) mainly verify the validity of this conclusion.

Without loss of generality, in order to verify the validity of the stability of the trivial response as well as the effectiveness of the damping described by equation (37), direct numerical integration of the linear parts of equation (19) has been made under three exciting conditions for its first mode when $\gamma = 0{\cdot}01$, i.e., (σ_ξ^2, σ_1) is taken to be (0·0002, 0), (0·0004, 0), or (0·0008, 0) respectively. Since the higher modes ($k \geqslant 2$) are neither directly

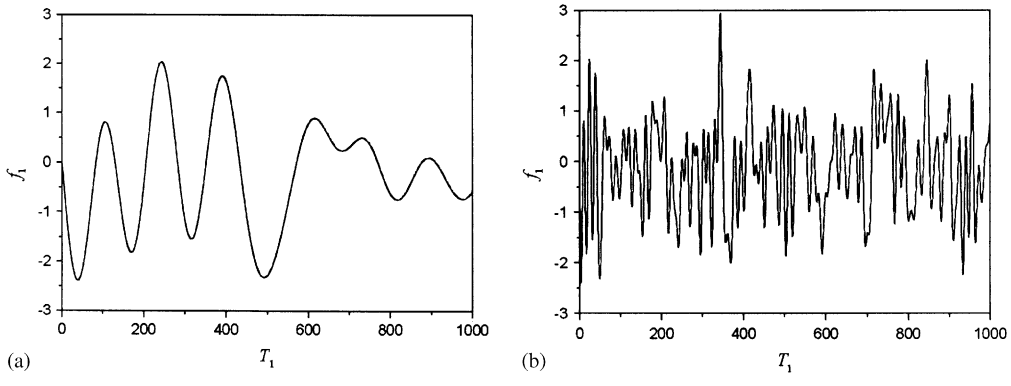

Figure 3. Time history of f_1 with $\sigma_\xi^2 = 1$: (a) $\gamma = 0{\cdot}01$; (b) $\gamma = 0{\cdot}1$.

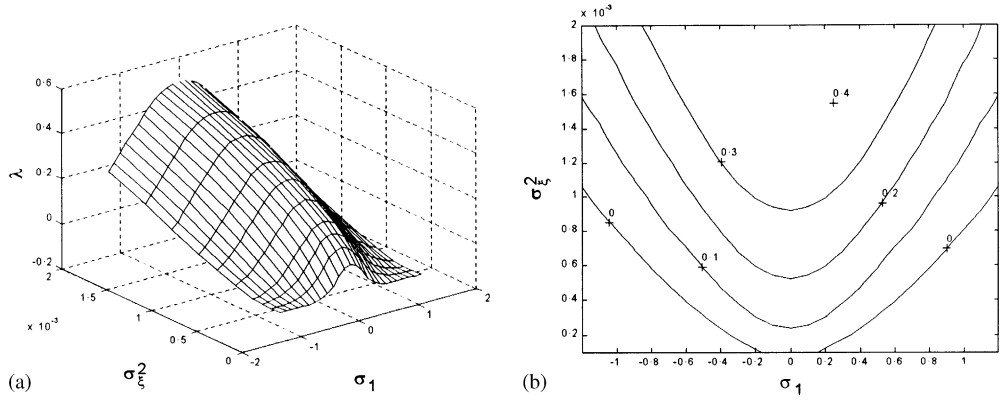

Figure 4. Largest Lyapunov exponent λ of the trivial response of the system to principal parametric resonance of its first mode: $\gamma = 0{\cdot}01$, $\hat{\varsigma}_1 = 0{\cdot}1$. (a) Mesh surface of $\lambda - (\sigma_1, \sigma_\xi^2)$; (b) isohypse curves of λ.

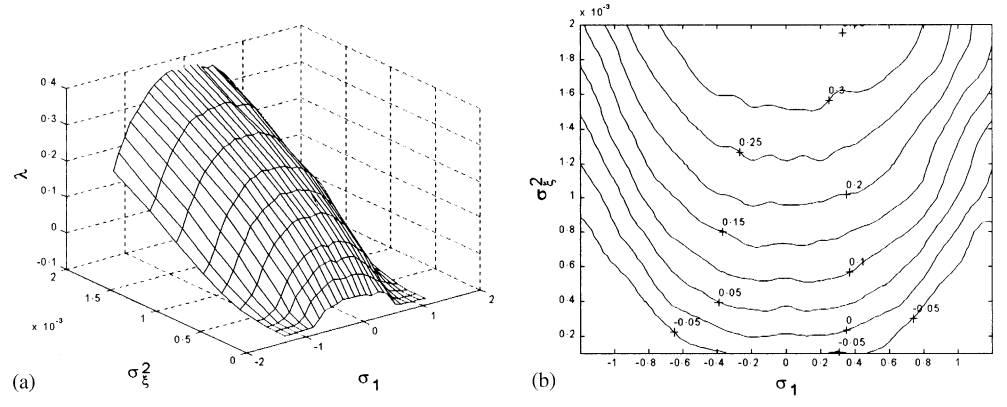

Figure 5. Largest Lyapunov exponent λ of the trivial response of the system to principal parametric resonance of its first mode: $\gamma = 0{\cdot}1$, $\hat{\varsigma}_1 = 0{\cdot}1$. (a) Mesh surface of $\lambda - (\sigma_1, \sigma_\xi^2)$; (b) isohypse curves of λ.

excited by parametric excitation nor indirectly excited by internal excitation, from the linear parts of equation (19) it can be shown that the response amplitude of these modes die out due to the presence of damping, and the response of the first mode can be solved independently. According to Figure 4(b), one can find that the exciting position of $(\sigma_\xi^2, \sigma_1) = (0{\cdot}0002, 0)$ in the $\sigma_\xi^2 - \sigma_1$ plane is between the isohypse curve $\lambda = 0$ and the isohypse curve $\lambda = 0{\cdot}1$, position of $(\sigma_\xi^2, \sigma_1) = (0{\cdot}0004, 0)$ between $\lambda = 0{\cdot}1$ and $0{\cdot}2$, and position of $(\sigma_\xi^2, \sigma_1) = (0{\cdot}0008, 0)$ between $\lambda = 0{\cdot}2$ and $0{\cdot}3$ respectively.

Figures 6(a)–(f) show the corresponding numerical integration results for the three exciting conditions stated above with different dumping parameters, where the initial integrating condition is chosen to be $(y_{10}, \dot{y}_{10}) = (0, 10)$. According to Figure 4(b), conditions in Figures 6(a), 6(c), and 6(e) will make the trivial response unstable and conditions in Figures 6(b), 6(d), and 6(f) will make it stable. Finally, one can find that the results in Figure 4(b) are in full agreement with that in Figure 6.

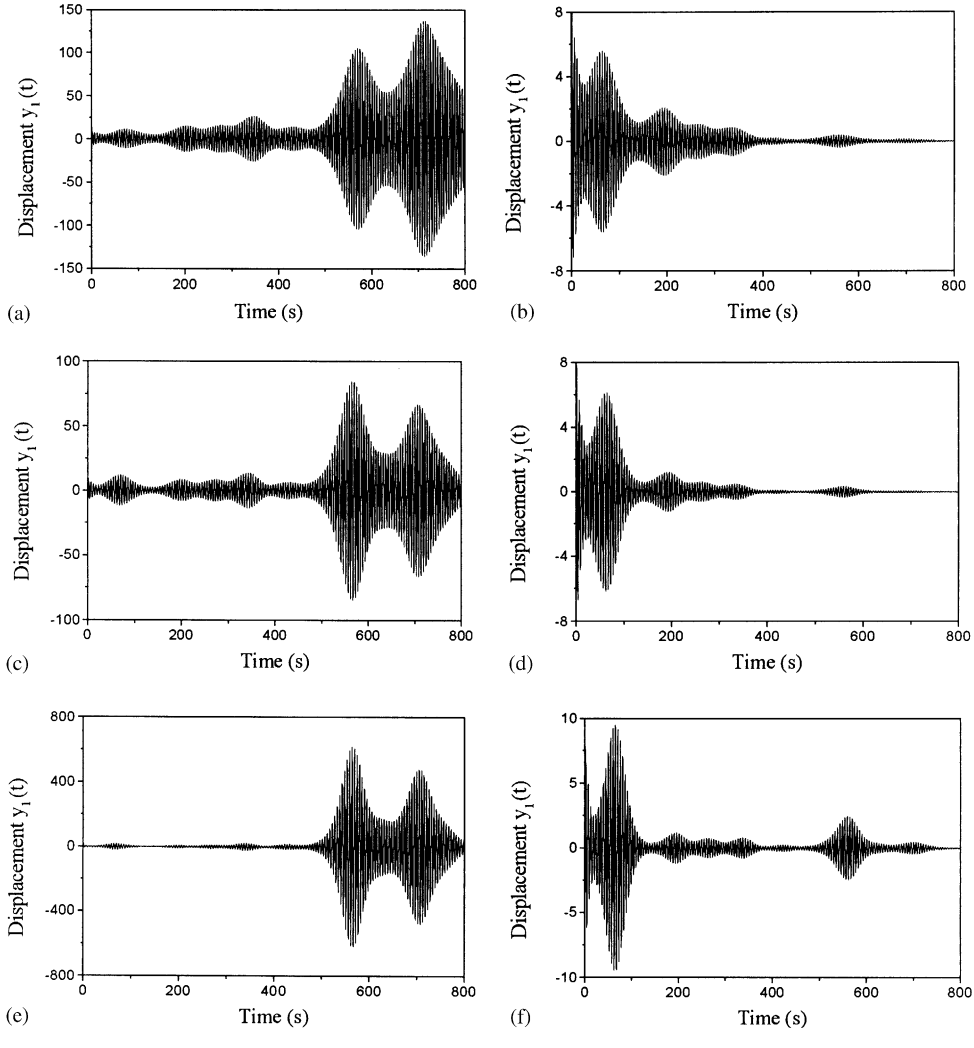

Figure 6. Numerical integration results for different exciting conditions: (a) $(\sigma_\xi^2, \sigma_1) = (0{\cdot}0002, 0)$, $\hat{\varsigma}_1 = 0{\cdot}1$; (b) $(\sigma_\xi^2, \sigma_1) = (0{\cdot}0002, 0)$, $\hat{\varsigma}_1 = 0{\cdot}2$; (c) $(\sigma_\xi^2, \sigma_1) = (0{\cdot}0004, 0)$, $\hat{\varsigma}_1 = 0{\cdot}2$; (d) $(\sigma_\xi^2, \sigma_1) = (0{\cdot}0004, 0)$, $\hat{\varsigma}_1 = 0{\cdot}3$; (e) $(\sigma_\xi^2, \sigma_1) = (0{\cdot}0008, 0)$, $\hat{\varsigma}_1 = 0{\cdot}3$; (f) $(\sigma_\xi^2, \sigma_1) = (0{\cdot}0008, 0)$, $\hat{\varsigma}_1 = 0{\cdot}4$.

4.2. COMBINATION RESONANCE OF THE FIRST TWO NATURAL MODES

4.2.1. *Modulation equations and the largest Lyapunov exponent*

Following equation (25), the condition of combination resonance between the first two natural modes holds true when $m = 1$ and $n = 2$, i.e., $\omega = \omega_1 + \omega_2 + \varepsilon\sigma_1$. Consequently, one obtains

$$2\mathrm{i}\omega_1(\hat{\varsigma}_1 A_1 + A_1') - \tfrac{1}{2}(\hat{f}_{22}^1 - \mathrm{i}\hat{g}_{22}^1)\bar{A}_2 \exp(\mathrm{i}\sigma_1 T_1) + c_{12}A_2\bar{A}_2 A_1 + c_{11}A_1^2\bar{A}_1 = 0,$$
$$2\mathrm{i}\omega_2(\hat{\varsigma}_2 A_2 + A_2') - \tfrac{1}{2}(\hat{f}_{22}^2 - \mathrm{i}\hat{g}_{22}^2)\bar{A}_1 \exp(\mathrm{i}\sigma_1 T_1) + c_{22}A_2^2\bar{A}_2 + c_{21}A_1\bar{A}_1 A_2 = 0. \quad (40)$$

Similarly, substituting the Cartesian transformation

$$A_k(T_1) = \tfrac{1}{2}[U_k(T_1) - \mathrm{i}V_k(T_1)]\,\mathrm{e}^{\mathrm{i}\lambda_1}, \quad \lambda_1 = \frac{\sigma_1}{2}T_1, \quad k = 1, 2 \quad (41)$$

into equation (40) and separating the results into real and imaginary parts, one arrives at a set of ordinary differential equations, namely, the modulation equations of steady state response:

$$\begin{aligned}
U_1' &= -\hat{\varsigma}_1 U_1 - \tfrac{1}{2}\sigma_1 V_1 - \frac{\hat{g}_{22}^1}{4\omega_1} U_2 + \frac{\hat{f}_{22}^1}{4\omega_1} V_2 + \frac{V_1}{8\omega_1} \sum_{k=1}^{2} c_{1k}(U_k^2 + V_k^2),\\
V_1' &= \tfrac{1}{2}\sigma_1 U_1 - \hat{\varsigma}_2 V_1 + \frac{\hat{f}_{22}^1}{4\omega_1} U_2 + \frac{\hat{g}_{22}^1}{4\omega_1} V_2 - \frac{U_1}{8\omega_1} \sum_{k=1}^{2} c_{1k}(U_k^2 + V_k^2),\\
U_2' &= -\frac{\hat{g}_{21}^2}{4\omega_2} U_1 + \frac{\hat{f}_{21}^2}{4\omega_2} V_1 - \hat{\varsigma}_2 U_2 - \tfrac{1}{2}\sigma_1 V_2 + \frac{V_2}{8\omega_2} \sum_{k=1}^{2} c_{2k}(U_k^2 + V_k^2),\\
V_2' &= \frac{\hat{f}_{21}^2}{4\omega_2} U_1 + \frac{\hat{g}_{21}^2}{4\omega_1} V_1 + \tfrac{1}{2}\sigma_1 U_2 - \hat{\varsigma}_2 V_2 - \frac{U_2}{8\omega_2} \sum_{k=1}^{2} c_{2k}(U_k^2 + V_k^2).
\end{aligned} \tag{42}$$

Substituting the following polar co-ordinate transformation [12]

$$U_1 = r\cos x\cos z, \quad V_1 = -r\sin x\cos z, \quad U_2 = r\cos y\sin z, \quad V_2 = -r\sin y\sin z \tag{43}$$

into the linear parts of equation (42), one can obtain a set of equations similar to equation (36) (see Appendix A), where r stands for the amplitude of the response of the system, x and y are the polar angles of the two sub-systems, respectively, and z is the coupling angle between the two sub-systems. However, it will result in failure for one to numerically simulate the largest Lyapunov exponent of the trivial response of the system owing to z crossing $n\pi/2$ ($n = 0, \pm 1, \pm 2, \ldots$). In what follows, therefore, one method for calculating the largest Lyapunov exponent of the trivial response of equation (42) is adopted [13], namely,

$$\lambda \approx \frac{1}{KT} \sum_{k=1}^{K} \ln\|\tilde{w}(kT)\|, \tag{44}$$

where T is generally chosen to be 10-fold the longest period of the linear system in question, K a larger number to ensure the stability of the numerically simulating results, $\tilde{w}(kT)$ the solution vector at $t = kT$, which is calculated with an initial condition of normalized $\tilde{w}(kT - T)$ and within an integrating period of $[(k-1)T, kT]$, and $\|\tilde{w}(kT)\|$ the modulus $\tilde{w}(kT)$.

In order to justify equation (44), the largest Lyapunov exponent λ and the corresponding isohypse curves of λ, which are determined by equation (44), are shown in Figures 7(a) and 7(b) with the same conditions as that in Figure 4, where $T = 90$ and $K = 30$. Comparison has been made between Figures 4 and 7 and the results show that they are almost the same.

4.2.2. *Numerical simulation of the largest Lyapunov exponent*

In the following simulation of the largest Lyapunov exponent of the trivial response, since a is fixed at 0·0912, all other parameters are kept the same as that in the last section but $\hat{f}_{22}^1 = \hat{f}_{21}^2 = 44{\cdot}46 f_1$ and $\hat{g}_{22}^1 = \hat{g}_{21}^2 = 44{\cdot}46 g_1$ should be added owing to the need of combination resonance analysis. After investigating and calculating the trivial response of equation (42), the parameters in equation (44) are finally chosen as follows: $T = 100$, $K = 30$. The variation of the largest Lyapunov exponent λ determined by equation (44) with σ_ξ^2 and σ_1 is shown in Figure 8(a) as $\lambda - (\sigma_1, \sigma_\xi^2)$ surface for the case of $\gamma = 0{\cdot}1$ and $\hat{\varsigma}_1 = \hat{\varsigma}_2 = 0{\cdot}1$. The corresponding isohypse curves of λ are shown in Figure 8(b).

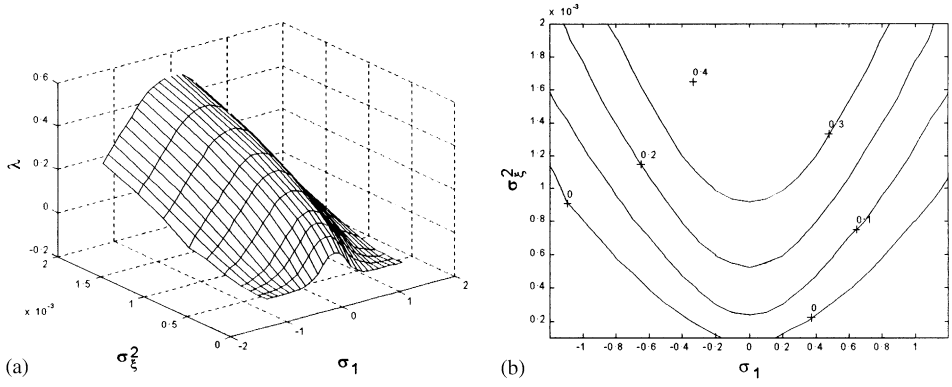

Figure 7. Largest Lyapunov exponent λ of the trivial response of the system to principal parametric resonance of its first mode calculated by equation (44): $\gamma = 0{\cdot}01$, $\hat{\varsigma}_1 = 0{\cdot}1$. (a) Mesh surface of $\lambda - (\sigma_1, \sigma_\xi^2)$; (b) isohypse curves of λ.

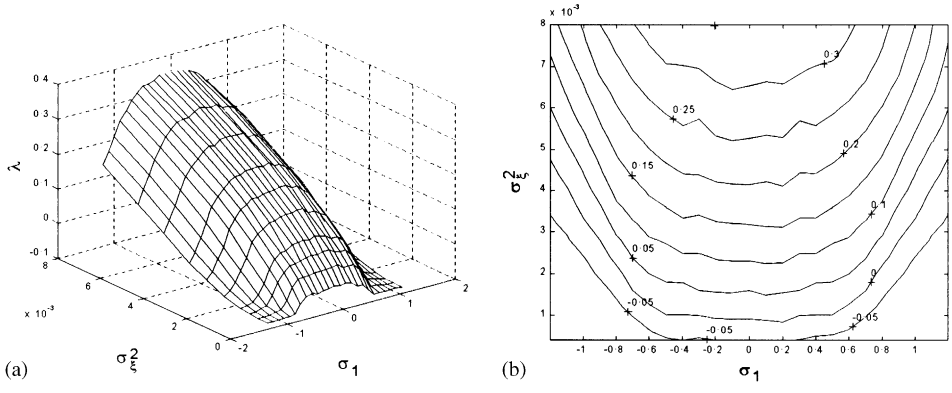

Figure 8. Largest Lyapunov exponent λ of the trivial response of the system to combination parametric resonance of its first two natural modes: $\gamma = 0{\cdot}1$, $\hat{\varsigma}_1 = \hat{\varsigma}_2 = 0{\cdot}1$. (a) Mesh surface of $\lambda - (\sigma_1, \sigma_\xi^2)$; (b) isohypse curves of λ.

Figures 8(a) and 8(b) correspond to Figures 5(a) and 5(b), respectively, and they have a similar contour, but the former will receive a stronger excitation than the latter for the same unstable area. In other words, the unstable area under the condition of combination parametric resonance of the first two natural modes will be narrower than that of the principal parametric resonance of the first mode if all parameters are kept the same.

5. RANDOM PARAMETRIC EXCITATION COMBINED WITH 3:1 INTERNAL RESONANCE BETWEEN THE FIRST TWO NATURAL MODES

As stated above, when a comes close to 0·3160, the condition of 3:1 internal resonance between the first two natural modes will hold true which results in that the two modes will be excited together no matter which is parametrically excited. Without loss of generality, in what follows, the principal parametric resonance of the first natural mode is investigated.

5.1. MODULATION EQUATIONS AND THE LARGEST LYAPUNOV EXPONENT

To describe the closeness of the beam to these two types of resonances, two detuning parameters are introduced as given below:

$$\omega = 2\omega_1 + \varepsilon\sigma_1, \quad \omega_2 = 3\omega_1 + \varepsilon\sigma_2. \tag{45}$$

Substituting these into equation (21b) yields

$$\begin{aligned}
&2\mathrm{i}\omega_1(\hat{\varsigma}_1 A_1 + A_1') - \tfrac{1}{2}[(\hat{f}^1_{21} - \mathrm{i}\hat{g}^1_{21})\bar{A}_1 \exp(\mathrm{i}\sigma_1 T_1) + (\hat{f}^1_{22} - \mathrm{i}\hat{g}^1_{22})]A_2 \exp\{\mathrm{i}(\sigma_2 - \sigma_1)T_1\}] \\
&\quad + \sum\nolimits_{j=1}^{n_2} c_{1j} A_j \bar{A}_j A_1 + d_{12} A_2 \bar{A}_1^2 \exp(\mathrm{i}\sigma_2 T_1) = 0, \\
&2\mathrm{i}\omega_2(\hat{\varsigma}_2 A_2 + A_2') - \tfrac{1}{2}(\hat{f}^2_{21} - \mathrm{i}\hat{g}^2_{21})A_1 \exp\{\mathrm{i}(\sigma_1 - \sigma_2)T_1\} + \sum\nolimits_{j=1}^{n_2} c_{2j} A_j \bar{A}_j A_2 \\
&\quad + d_{21} A_1^3 \exp(-\mathrm{i}\sigma_2 T_1) = 0,
\end{aligned} \tag{46}$$

where $d_{12} = \hat{\alpha}^1_{121} + \hat{\alpha}^1_{211} + \hat{\alpha}^1_{112} - 2\omega_1^2\hat{\beta}^1_{211} + \omega_1\omega_2(\hat{\beta}^1_{121} + \hat{\beta}^1_{112}) - (\omega_1^2\hat{\beta}^1_{121} + \omega_2^2\hat{\beta}^1_{112})$ and $d_{21} = \hat{\alpha}^2_{111} - 2\omega_1^2\hat{\beta}^2_{111}$.

Similar to equation (40), substituting the Cartesian transformation

$$A_k(T_1) = \tfrac{1}{2}[U_k(T_1) - \mathrm{i}V_k(T_1)]\,\mathrm{e}^{\mathrm{i}\lambda_k}, \quad k = 1, 2 \quad \lambda_1 = \frac{\sigma_1}{2}T_1, \quad \lambda_2 = \left(\tfrac{3}{2}\sigma_1 - \sigma_2\right)T_1 \tag{47}$$

into equation (46) and separating the results into real and imaginary parts, one finally has

$$\begin{aligned}
U' = &-\left(\hat{\varsigma}_1 + \frac{\hat{g}^1_{21}}{4\omega_1}\right)U_1 - \frac{1}{2}\left(\sigma_1 - \frac{\hat{f}^1_{21}}{2\omega_1}\right)V_1 - \frac{\hat{g}^1_{22}}{4\omega_1}U_2 - \frac{\hat{f}^1_{22}}{4\omega_1}V_2 + \frac{V_1}{8\omega_1}\sum\nolimits_{i=1}^{2} c_{1i}(U_i^2 + V_i^2) \\
&- \frac{1}{8\omega_1}d_{12}[V_2(V_1^2 - U_1^2) + 2U_1V_1U_2], \\
V' = &\frac{1}{2}\left(\sigma_1 + \frac{\hat{f}^1_{21}}{2\omega_1}\right)U_1 - \left(\hat{\varsigma}_1 - \frac{\hat{g}^1_{21}}{4\omega_1}\right)V_1 + \frac{\hat{f}^1_{22}}{4\omega_1}U_2 - \frac{\hat{g}^1_{22}}{4\omega_1}V_2 - \frac{U_1}{8\omega_1}\sum\nolimits_{i=1}^{2} c_{1i}(U_i^2 + V_i^2) \\
&- \frac{1}{8\omega_1}d_{12}[U_2(U_1^2 - V_1^2) + 2U_1V_1V_2], \\
U_2' = &-\frac{\hat{g}^2_{21}}{4\omega_2}U_1 - \frac{\hat{f}^2_{21}}{4\omega_2}V_1 - \hat{\varsigma}_2 U_2 - \tfrac{1}{2}(3\sigma_1 - 2\sigma_2)V_2 + \frac{V_2}{8\omega_2}\sum\nolimits_{i=1}^{2} c_{2i}(U_i^2 + V_i^2) \\
&+ \frac{1}{8\omega_2}d_{21}V_1(3U_1^2 - V_1^2), \\
V_2' = &\frac{\hat{f}^2_{21}}{4\omega_2}U_1 - \frac{\hat{g}^2_{21}}{4\omega_2}V_1 + \tfrac{1}{2}(3\sigma_1 - 2\sigma_2)U_2 - \hat{\varsigma}_2 V_2 - \frac{U_2}{8\omega_2}\sum\nolimits_{i=1}^{2} c_{2i}(U_i^2 + V_i^2) \\
&- \frac{1}{8\omega_2}d_{21}U_1(U_1^2 - 3V_1^2).
\end{aligned} \tag{48}$$

To numerically simulate the largest Lyapunov exponent of the trivial response of equation (48), equation (44) is used again. Also, the polar co-ordinate transformation of the linear parts of equation (48) can be seen in Appendix B.

TABLE 1

Internal resonance tuning parameter and the corresponding coefficients

a	σ_2	ω_1	ω_2	$\hat{f}_{21}^1$	$\hat{g}_{21}^1$	$\hat{f}_{22}^1$	$\hat{g}_{22}^1$	$\hat{f}_{21}^2$	$\hat{g}_{21}^2$
0·3643	−1	1·6334	4·8001	$43{\cdot}17f_1$	$43{\cdot}17g_1$	$32{\cdot}20f_1$	$32{\cdot}20g_1$	$32{\cdot}20f_1$	$32{\cdot}20g_1$
0·3160	0	1·5679	4·7037	$43{\cdot}71f_1$	$43{\cdot}71g_1$	$33{\cdot}46f_1$	$33{\cdot}46g_1$	$33{\cdot}46f_1$	$33{\cdot}46g_1$
0·2715	1	1·5042	4·6126	$44{\cdot}23f_1$	$44{\cdot}23g_1$	$34{\cdot}69f_1$	$34{\cdot}69g_1$	$34{\cdot}69f_1$	$34{\cdot}69g_1$

5.2. NUMERICAL SIMULATION OF THE LARGEST LYAPUNOV EXPONENT

To understand well the stability of the slender beam subject to random principal parametric resonance combined with internal resonance, a few case studies at different movements are given in this section. In Table 1, the internal resonance turning parameter σ_2 and the corresponding coefficients are listed for three values of a.

The variations of the largest Lyapunov exponent λ determined by equation (48) with σ_ξ^2 and σ_1 are shown in Figures 9(a), 9(c), and 9(e) as $\lambda - (\sigma_1, \sigma_\xi^2)$ surface for the case of $\gamma = 0{\cdot}01$, $\sigma_2 = -1$, 0 and 1, and $\hat{\varsigma}_1 = \hat{\varsigma}_2 = 0{\cdot}05$ respectively. The corresponding isohypse curves of λ are shown in Figures 9(b), 9(d), 9(f) respectively. One can find that there is a principal ridge in Figures 9(a), 9(c), and 9(e), respectively, which almost has the same shape and size in the three figures, owing to the principal resonance. However, near the principal ridge three exists a subordinate ridge, which moves from the left of the principal one (see Figure 9(a)) to the right of it (see Figure 9(e)) when σ_2 increases from the negative to the positive and perfectly covered by the principal one when $\sigma_2 = 0$ (see Figure 9(c)), owing to the presence of internal resonance. Also, the changes of the shape and the size of the almost certain unstable regions for the trivial response can be determined by the zero-isohypse curves in Figures 9(b), 9(d), and 9(f). These curves are similar to that for the sinusoidal case [2].

Figures 10(a) and 10(b) correspond to Figures 9(a) and 9(b) respectively. All parameters except the parametric excitation bandwidth γ are kept the same: γ is increased from 0·01 to 0·1. It can be seen in Figure 10(a) that the increase of the bandwidth results in a rapid decrease of λ in the area of principal resonance and the principal ridge becomes flatter. More especially, the subordinate ridge has disappeared due to the increase of the bandwidth. Also, the zero-isohypse curve in Figure 10(b) indicates that the almost certain unstable region is narrower than that in Figure 9(b) and the presence of the internal resonance influences the stability of the trivial response next to nothing. From this point of view, it can be concluded that the increase of γ is beneficial to the stability of the trivial response of the system and can suppress the instability arising from internal resonance effectively.

6. CONCLUSIONS

The largest Lyapunov exponent of the trivial response for a simply supported beam under a large linear motion of basement increases rapidly when either the principal parametric resonance or the combination parametric resonance is excited by a narrowband random noise, which may result in the almost certain instability of the system. Moreover, when the case of the principal parametric resonance of the first natural mode of the system combined with 3:1 internal resonance between the first two natural modes of it holds true, there exists not only a principal ridge but also a subordinate ridge

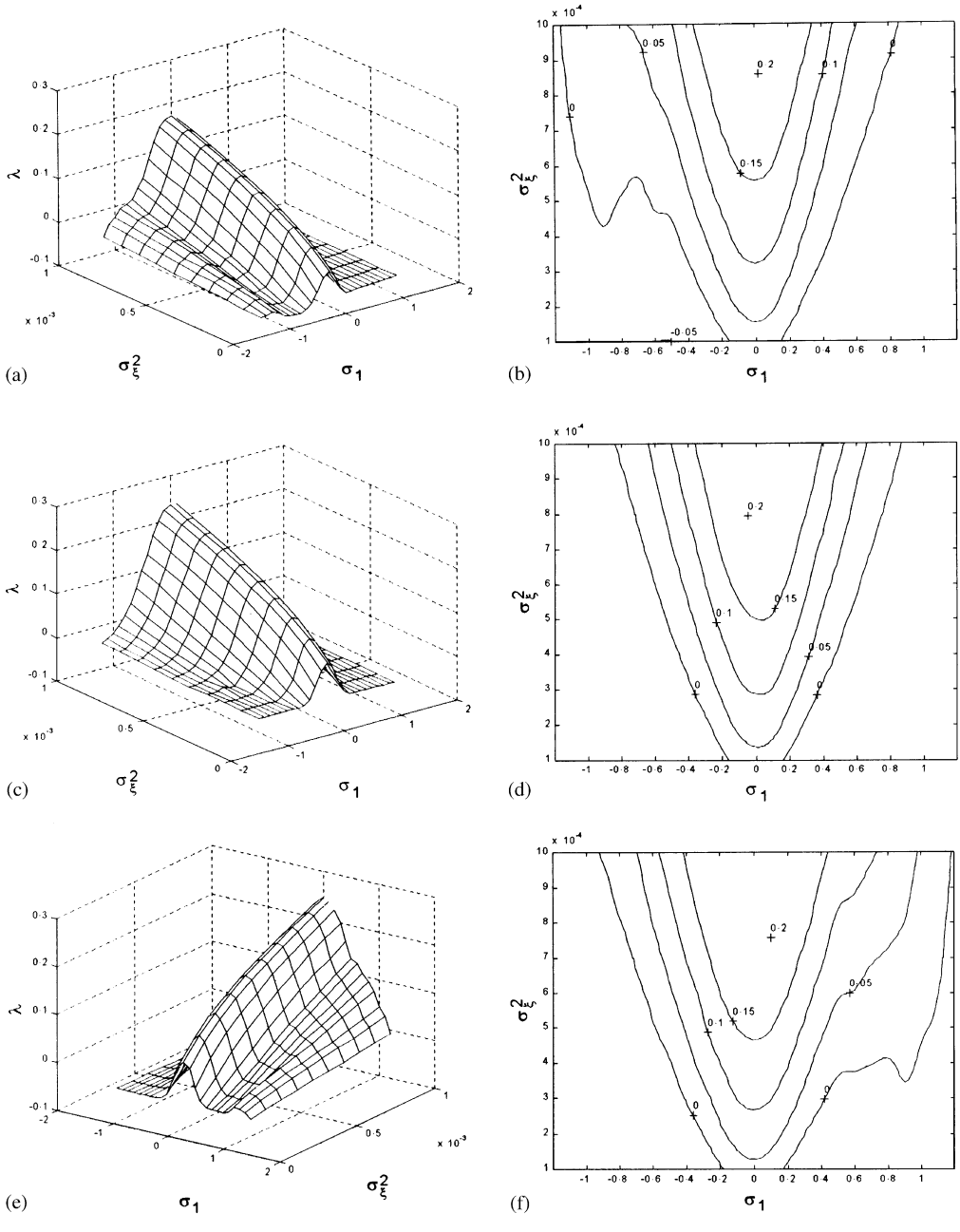

Figure 9. Largest Lyapunov exponent λ of the trivial response of the system to principal parametric resonance of its first natural mode combined with 3:1 internal resonance of its first two natural modes: $\gamma = 0{\cdot}01$, $\hat{\varsigma}_1 = \hat{\varsigma}_2 = 0{\cdot}05$. (a, b) $\sigma_2 = -1$; (c, d) $\sigma_2 = 0$; (e, f) $\sigma_2 = 1$. (a, c, e) Mesh surface of $\lambda - (\sigma_1, \sigma_\xi^2)$; (b, d, f) isohypse curves of λ.

near the principal one on $\lambda - (\sigma_1, \sigma_\xi^2)$ surface. Numerical results show that the subordinate ridge is closely related to the internal resonance frequency detuning parameter σ_2. The wider the bandwidth of the narrowband random excitation is, the flatter the principal ridge becomes and the more possible the disappearance of the subordinate ridge is. On the

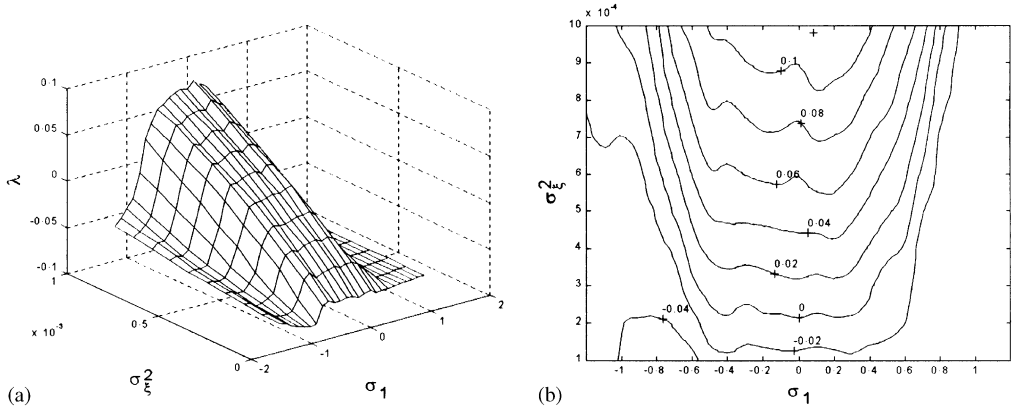

Figure 10. Largest Lyapunov exponent λ of the trivial response of the system to principal parametric resonance of its first natural mode combined with 3:1 internal resonance of its first two natural modes: $\gamma = 0{\cdot}1$, $\hat{\varsigma}_1 = \hat{\varsigma}_2 = 0{\cdot}05$, $\sigma_2 = -1$. (a) Mesh surface of $\lambda - (\sigma_1, \sigma_\xi^2)$; (b) isohypse curves of λ.

other hand, the isohypse curves indicate that the increase of the damping of the system can effectively lessen the instability area of the trivial response. The validity of the almost certain stability obtained by means of the method of multiple scales is verified by direct numerical integration of the equation of motion of the system.

REFERENCES

1. Z. H. Feng and H. Y. Hu 2002 *Acta Mechanica Solida Sinica*. **15**, 133–139. Nonlinear dynamic modeling and periodic vibration of a cantilever beam subjected to axial movement of basement.
2. Z. H. Feng and H. Y. Hu 2002 *Acta Mechanica Sinica* **34**, 389–400. Dynamic stability analysis of a slender beam with internal resonances under a large linear motion.
3. S. Rajan and H. G. Davies 1988 *Journal of Sound and Vibration* **123**, 497–506. Multiple time scaling of the response of a Duffing oscillator to narrow-band random excitation.
4. H. G. Davies and S. Rajan 1988 *Journal of Sound and Vibration* **126**, 195–208. Random superharmonic and subharmonic response: multiple time scaling of a Duffing oscillator.
5. A. H. Nayfeh and S. J. Serhan 1990 *International Journal of Non-Linear Mechanics* **25**, 493–509. Response statistics of non-linear systems to combined deterministic and random excitations.
6. W. Q. Zhu, M. Q. Lu and Q. T. Wu 1993 *Journal of Sound and Vibration* **165**, 285–304. Stochastic jump and bifurcation of a Duffing oscillator under narrow-band excitation.
7. W. Q. Zhu 1992 *Random Vibration*. Beijing: Science Press.
8. H. W. Rong, W. Xu and T. Fang 1998 *Acta Mechanica Sinica* **30**, 178–185. Principal response of Duffing oscillator to combined deterministic and narrow-band random parametric excitation.
9. H. Rong, W. Xu and T. Fang 1998 *Journal of Sound and Vibration* **210**, 483–515. Principal response of Duffing oscillator to combined deterministic and narrow-band random parametric excitation.
10. R. L. Stratonovich 1963 *Topics in the Theory of Random Noise*. New York: Gordon & Breach.
11. S. H. Shinozuka 1971 *Journal of the Acoustical Society of America* **49**, 357–367. Simulation of multivariate and multidimensional random processes.
12. H. W. Rong, W. Xu and T. Fang 1998 *Chinese Journal of Applied Mechanics* **15**, 22–29. Maximal Lyapunov exponent and almost-sure sample stability for coupled two-degree-of-freedoms nonlinear stochastic systems.
13. H. Y. Hu 2000 *Applied Nonlinear Dynamics*. Beijing: Aviation Industry Press.

APPENDIX A

The polar co-ordinate form of the linear parts in equation (42) transformed by using equation (43):

$$r' = -\frac{r}{2}(\hat{\varsigma}_1 + \hat{\varsigma}_2) + \frac{r}{16\omega_1\omega_2}[(\omega_1\hat{f}^2_{21} + \omega_2\hat{f}^1_{22})\{\cos(x+2z+y) - \cos(x-2z+y)\} + (\omega_1\hat{g}^2_{21} + \omega_2\hat{g}^1_{22})\{\sin(x-2z+y) - \sin(x+2z+y)\} + 8\omega_1\omega_2(\hat{\varsigma}_2 - \hat{\varsigma}_1)\cos(2z)], \tag{A1}$$

$$x' = \frac{1}{8\omega_1\cos z}[-4\omega_1\sigma_1\cos z - \hat{g}^1_{22}\cos(x+y+z) + \hat{g}^1_{22}\cos(x+y-z) - \hat{f}^1_{22}\sin(x+y+z) + \hat{f}^1_{22}\sin(x+y-z)], \tag{A2}$$

$$y' = \frac{1}{8\omega_2\sin z}[-4\omega_2\sigma_1\sin z - \hat{g}^2_{21}\sin(x+y+z) + \hat{g}^2_{21}\sin(x+y-z) - \hat{f}^2_{21}\cos(x+y+z) - \hat{f}^2_{21}\cos(x+y-z)], \tag{A3}$$

$$z' = \frac{\sin(2z)}{2}(\hat{\varsigma}_1 - \hat{\varsigma}_2) + \frac{1}{16\omega_1\omega_2}[-(\omega_1\hat{g}^2_{21} + \omega_2\hat{g}^1_{22})\{\cos(x+2z+y) + \cos(x-2z+y)\} + (\omega_1\hat{f}^2_{21} + \omega_2\hat{f}^1_{22}))\sin(x+2z+y) + \sin(x-2z+y)\} + 2(\omega_1\hat{f}^2_{21} - \omega_2\hat{f}^1_{22})\sin(x+y) - 2(\omega_1\hat{g}^2_{21} + \omega_2\hat{g}^1_{22})\cos(x+y)]. \tag{A4}$$

APPENDIX B

The polar co-ordinate form of the linear parts in equation (48) transformed by equation (43):

$$r' = -\frac{r}{2}(\hat{\varsigma}_1 + \hat{\varsigma}_2) + \frac{r}{16\omega_1\omega_2}[(\omega_1\hat{g}^2_{21} + \omega_2\hat{g}^1_{22})\{\sin(x-2z-y) - \sin(x+2z-y)\} + (\omega_1\hat{f}^2_{21} - \omega_2\hat{f}^1_{22})\{\cos(x-2z+y) - \cos(x+2z-y)\} - \omega_2\hat{g}^1_{21}\{\cos(2x-2z) + \cos(2x+2z)\} + 8\omega_1\omega_2(\hat{\varsigma}_2 - \hat{\varsigma}_1)\cos(2z) - \omega_2\hat{f}^1_{21}\{\sin(2x-2z) + \sin(2x+2z)\} - 2\omega_2\hat{f}^1_{21}\sin(2x) - 2\omega_2\hat{g}^1_{21}\cos(2x)], \tag{B1}$$

$$y' = \frac{1}{8\omega_1\cos z}[-4\omega_1\sigma_1\cos z + \hat{g}^1_{22}\cos(x-y-z) - \hat{g}^1_{22}\cos(x-y+z) + \hat{f}^1_{22}\sin(x-y-z) - \hat{f}^1_{22}\sin(x-y+z) + 2g^1_{21}\{\sin(2x-z) + \sin(2x+z)\} - 2\hat{f}^1_{21}\{\cos(2x-z) + \cos(2x+z)\}], \tag{B2}$$

$$y' = \frac{1}{8\omega_2 \sin z}[(8\sigma_2 - 12\sigma_1)\omega_2 \sin z - \hat{g}_{21}^2 \sin(x - y - z) - \hat{g}_{21}^2 \sin(x - y + z) - \hat{f}_{21}^2 \cos(x - y - z) - \hat{f}_{21}^2 \cos(x - y + z)], \tag{B3}$$

$$z' = \frac{\sin(2z)}{2}(\hat{\varsigma}_1 - \hat{\varsigma}_2) + \frac{1}{16\omega_1\omega_2}[-(\omega_1\hat{g}_{21}^2 + \omega_2\hat{g}_{22}^1)\{\cos(x + 2z - y) + \cos(x - 2z - y)\} + (\omega_1\hat{f}_{21}^2 - \omega_2\hat{f}_{22}^1)\{\sin(x + 2z - y) + \sin(x - 2z - y)\} + 2(\omega_1\hat{f}_{21}^2 - \omega_2\hat{f}_{22}^1)\sin(x - y) - 2(\omega_1\hat{g}_{21}^2 - \omega_2\hat{g}_{22}^1)\cos(x - y) - \omega_2\hat{f}_{21}^1\{\cos(2x + 2z) - \cos(2x - 2z)\} - \omega_2\hat{g}_{21}^1\{\sin(2x - 2z) - \sin(2x + 2z)\}]. \tag{B4}$$